INTRINSIC FLOW BEHAVIOR IN A SLURRY BUBBLE COLUMN UNDER HIGH PRESSURE AND HIGH TEMPERATURE CONDITIONS

(Quarterly Report)

(Reporting Period: April 1 to June 30, 1996)

Liang-Shih Fan

DEPARTMENT OF CHEMICAL ENGINEERING
THE OHIO STATE UNIVERSITY
COLUMBUS, OHIO 43210

July 17, 1996

Prepared for Air Products and Chemicals, Inc.

WORK PERFORMED

1. *Measurement of liquid viscosity*

The experiments on liquid viscosity measurement were started two months ago. The experiments were conducted in the high pressure and temperature system, and nitrogen was used to pressurize the system. The molecular structures of Paratherm NF heat transfer fluid and other oganic liquid (e.g, mineral oil and F-T wax) are complex. There is no theoretical method to accurately estimate the viscosity of these liquid. Thus, direct measurements using such methods as falling ball and plate-and-cone or couette-type viscometers are the only alternative. In the direct measurement of liquid viscosity conducted in this study, falling ball technique was used to measure the viscosity of Paratherm NF heat transfer fluid. The Reynolds number based on the particle diameter is maintained in all experiments at less than 2 by varying the particle sizes. The Stokes (1851) and Oseen (1910) equations given below were applied to calculate the viscosity for different flow regimes, based on the Reynolds number:

$$\mu = f_w \frac{d_p^2(\rho_p - \rho_f) g \Delta t}{18L} \qquad (Re_t < 0.1) \tag{1}$$

$$\mu = f_w \frac{d_p^2(\rho_p - \rho_f) g \Delta t}{18L\,(1 + 3Re_t/16)} \qquad (0.1 < Re_t < 2) \tag{2}$$

where f_w is the correction factor accounting for the wall effect, and can be expressed by (Khan and Richardson, 1989)

$$f_w = 1 - 1.15(d_p/D)^{0.6} \tag{3}$$

Figure 1 shows the variations of the viscosity with pressure and temperature for Paratherm NF heat transfer fluid. The results were partially verified by comparing the measurements with values provided by the Paratherm supplier at a pressure of 0.1 MPa and temperatures below the boiling point. The differences between the measured values and the supplier's results are less than 1%.

In general, the liquid molecules move within parallel liquid layers, where they change their sites by surpassing the activation energy barrier (Ewell and Eyring, 1937). As the pressure increases at low temperatures, the liquid exerts a larger frictional drag on adjacent molecule layers, and the velocity gradient decreases, which causes the viscosity to increase significantly. For high temperatures, however, the liquid molecules have excess free energy to overcome the energy barrier, and thus an increase in pressure does not significantly affect the liquid viscosity. Figure 1 shows that when the pressure increases from 0.1 to 21 MPa, the viscosity for Paratherm NF heat transfer fluid increases by 65% at 20°C, but only by 10% at 100°C. Figure 1 also indicates that the effect of temperature on the liquid viscosity is more significant than that of pressure.

2. ***Bubble effects on the transient flow pattern in bubble columns***

For the flow in a two-dimensional (2-D) air-water bubble column of 15 cm in width at the superficial gas velocity of 1 cm/s, a time series of 322 consecutive vector fields was constructed by a Particle Image Velocimetry (PIV). The PIV technique has the capability to provide the transient, full-field behavior of a fluid flow without obstructing the flow. The series comprises 10.73 s of the flow and contains the passage of two vortices in the field of view. This analysis allows for the study of the flow dynamics in great detail (deterministic and stochastic properties). The profiles of the averaged horizontal and vertical liquid velocities, u and v, respectively; and Reynolds stresses were obtained from the liquid velocity fields as shown in Figures 2 and 3. The averaged vertical liquid flow consists of upward flow in the center of the column and downward flow adjacent to the sidewalls. The Reynolds normal stress in the horizontal direction peaks in the center, whereas the vertical normal stress has a local minimum in the center and maximum between the wall and the center. The Reynolds shear stress is proportional to the gradient of averaged vertical velocity profile suggesting a Boussinesq type of approximation. Furthermore, the Reynolds normal stresses are considerably greater than the Reynolds shear stress.

For each field, the liquid vectors were redistributed over a 10 by 10 grid. After the cell averaged velocities were computed for the entire 10.73 s series, they were subtracted from the instantaneous vectors in the respective cells. In Figures 4a and 4b, the series of both components for grid cell (3,5) are shown. It should be noted that the left lower cell within the field of view has coordinates (1,1). The vortical structures are clearly demonstrated, i.e. periods of positive and negative axial velocity alternate. Plots for the other grid cells look similar, with the exception of the cells adjacent to the walls where the horizontal velocity fluctuations are strongly damped and the center cells where the presence of the vortices is less dominant in the vertical velocity. Figure 5 shows the power spectral density functions of both u and v for grid cell (3,5). Again, the vortical structures dominate, i.e. hardly any power is found above 1 Hz even up to the Nyquist frequency of 15 Hz.

Cross-correlating of u-u for the cells on a horizontal row, i.e. with the same j-coordinate, reveals that the u-components are in phase. The cross-correlation indicates that the vortices span the entire column width and flow as one big entity into the field of view. Similarly, cross-correlating of v-v for a row shows that correlating of two cells at the same side of the column symmetry axis means zero-phase shift and at different sides gives 180°-phase shift. In the latter case different sides of the vortex were probed. Finally, from the cross-correlation between $v(2,2)$ and $v(2,j)$ with j = 1 to 10, a time shift, Δt, was found to increase with increasing distance, Δy, between the cells. In Figure 6 this time shift is plotted as a function of distance. Fitting a straight line through the data points gives a reasonable estimate of the descending velocity of the vortical structures. Note that the negative time shift means cell (2,2) responds later than cell $(2,j)$. The descending velocity of -5.5 cm/s was found which shows the vortical structures are moving downward.

The data from the time series demonstrate that the velocity field can be decomposed into a slow sine-like oscillation due to the passage of a vortex and 'high' frequency content associated with 'turbulence' as shown in Figures 4a and 4b. The power spectra support the use of only one sine-like carrier wave for the vortices with a frequency around 0.2 Hz. As mentioned, the flow field can be decomposed according to:

$$v(i,j,t) = \langle v(i,j) \rangle + a_{ij}\cos\left(2\pi f_{ij} t + \varphi_{ij}\right) + v_f(i,j,t) \tag{4}$$

where $v(i,j;t)$ is the vertical component of the velocity in grid cell (i,j); $\langle v(i,j)\rangle$ is its time-average; a_{ij}, f_{ij} and φ_{ij} are the amplitude, frequency and phase to be fitted, respectively; and $v_f(i,j;t)$ is the 'turbulent' part in grid cell (i,j). Now the Reynolds stresses can be recalculated using v_f as

$$\langle v'_f(i,j)v'_f(i,j)\rangle = \left(\frac{1}{322}\sum_{k=o}^{322} v_f(i,j,k)v_f(i,j,k)\right) - \langle v_f(i,j)\rangle^2 \tag{5}$$

The horizontal component of the velocity, u, and the other two stresses were treated similarly. The resultant stresses are shown in Figure 7. The figure shows the profiles for one grid row of $j = 5$. The figure demonstrates that removing the contribution of the vortices has a significant affect on the stresses. With the removal of the vortical structures, relatively flat normal stresses were obtained that have values close to the minimum in $\langle v'v'\rangle$. It can be concluded from this analysis, that the high frequency content of the normal stresses, i.e. the 'turbulence', has a rather flat profile with a magnitude of 50-100 cm^2/s^2.

3. *Gas holdup in high pressure and temperature bubble column*

The measurements of gas holdup in the high pressure and temperature bubble column with a porous plate distributor was carried out last quarter. The experiments were focused on the pressure effects under various gas velocities. Figure 8 shows the effect of pressure on the gas holdup in the liquid-batch bubble column. The value of the gas holdup is associated with the bubble rise velocity and the number density of bubbles in the system. The bubble rise velocity, in turn, depends on the bubble size and shape, physical properties of the liquid, and flow pattern. In Figure 8, the gas holdup is plotted against the superficial gas velocity for pressures varying from 0.1 to 20.4 MPa. It is seen that at low gas velocities, the gas holdup increases linearly with increasing gas velocity for all pressures. The significant pressure effects on the gas holdup were observed at high gas velocity conditions for pressures up to 10 MPa. At pressures higher than 10 MPa, the gas holdup is insensitive to the operating pressure for the gas velocity range examined in this study. Pressure effects on the gas holdup were reported also to be significant at high gas velocities by Idogawa et al. (1986) for a air-water system with pressures up to 5 MPa. The increase in the gas holdup with increasing pressure can be attributed to a decrease in bubble size and an increase in number density of bubbles. Visualization revealed that the increase in the gas holdup from pressures of 3.5 MPa to 20.5 MPa is due to an increase in the bubble number concentration since the mean bubble size is insensitive to the pressure in the current system. As noted earlier, there is no significant bubble interaction in the dispersed bubble regime, and thus the condition for the pressure effects on the gas holdup appears to be concerned with the process of bubble formation. As the gas velocity increases, bubbles of smaller size are formed with a higher formation frequency in the higher pressure system (Kling, 1962; Idogawa et al., 1987a), which results in a higher gas holdup compared to those in the system operated under atmospheric pressures.

WORK TO BE PERFORMED NEXT QUARTER

1. Quantitative analysis of the transient flow pattern in bubble columns will be continued next quarter with emphasis on the deterministic flow structure.
2. Gas holdup in the high pressure and temperature bubble column will be continued next quarter.

Notations

D	diameter of column (mm)
d_p	diameter of particle (mm)
f_w	correction factor for wall effect (-)
g	gravitational acceleration (m/s^2)
L	falling distance (m)
p	pressure (MPa)
Re	Reynolds number based on particle diameter $\rho_f u d_p/\mu$ (-)

Re_t Reynolds number based on particle diameter $\rho_f u_t d_p/\mu$ (-)

Greek letters

μ liquid viscosity (kg/m·s)

ρ_p particle density (kg/m^3)

ρ_f liquid density (kg/m^3)

REFERENCES

Ewell, R.H. and H. Eyring, "Theory of the Viscosity of Liquids as a Function of Temperature and Pressure," *J. Chem. Phys.*, **5**, 726 (1937).

Idogawa, K., K. Ikeda, T. Fukuda, and S. Morooka, S., "Behavior of bubbles of air-water system in a column under high pressure," *Inter. Chem. Eng.*, **26**, 468 (1986).

Idogawa, K., K. Ikeda, and T. Fukuda, "Formation and flow of gas bubbles in a pressurized bubble column with a single orifice or nozzle gas distributor," *Chem. Eng. Comm.*, **59**, 201 (1987a).

Khan, A.R. and J.F. Richardson, "Fluid-Particle Interactions and Flow Characteristics of Fluidized Beds and Settling Suspensions of Spherical Particles," *Chem. Eng. Comm.*, **78**, 111 (1989).

Kling, G., "Über die Dynamik der Blasenbildung Beim Begasen von Flüssigkeiten Unter Druck," *Inter. J. Heat Mass Transfer*, **5**, 211 (1962).

Oseen, C.W., "Über die Stokes'sche Formel und über eine verwandte Aufgabe in der Hydrodynamik," *Ark. Mat. Astron. Fys.*, **6**, 29 (1910).

Stokes, G.G., "On the effect of internal friction of fluids on the motion of pendulums," *Trans. Cambridge Phil. Soc.*, **9**, 8 (1851).

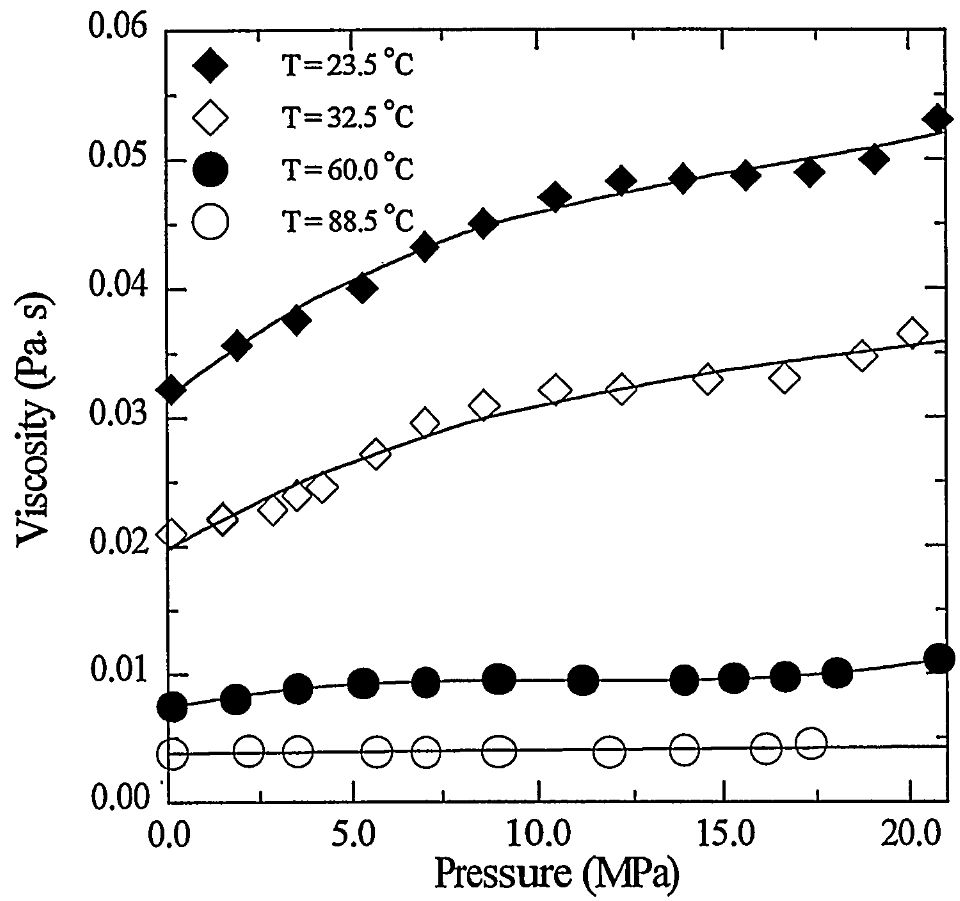

Figure 1. A preliminary study on the effects of pressures and temperatures on the viscosity of Paratherm NF heat transfer fluid

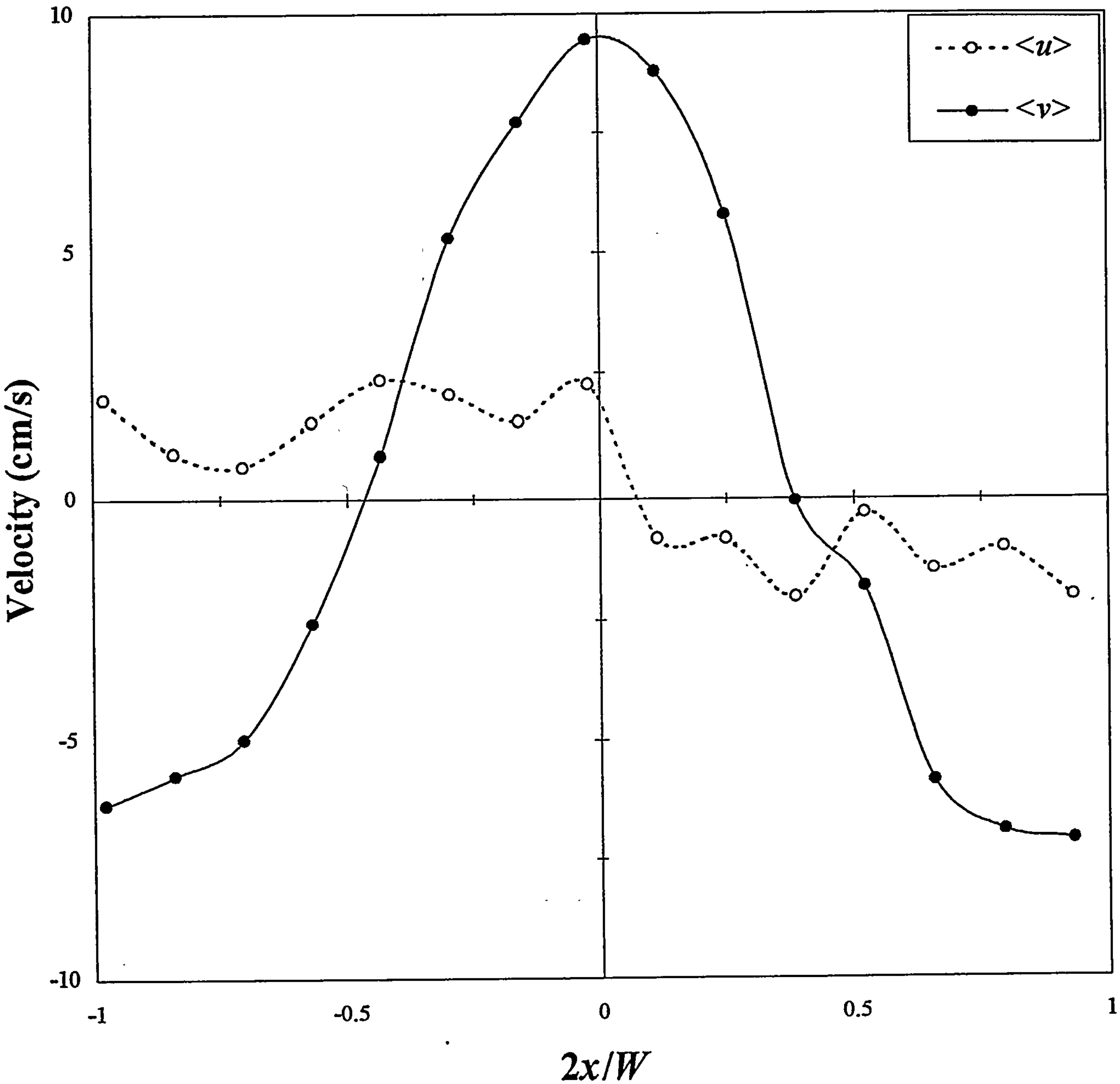

Figure 2. Averaged velocity profiles for the middle section of the 11 cm column at U_{sup} = 1.0 cm/s.

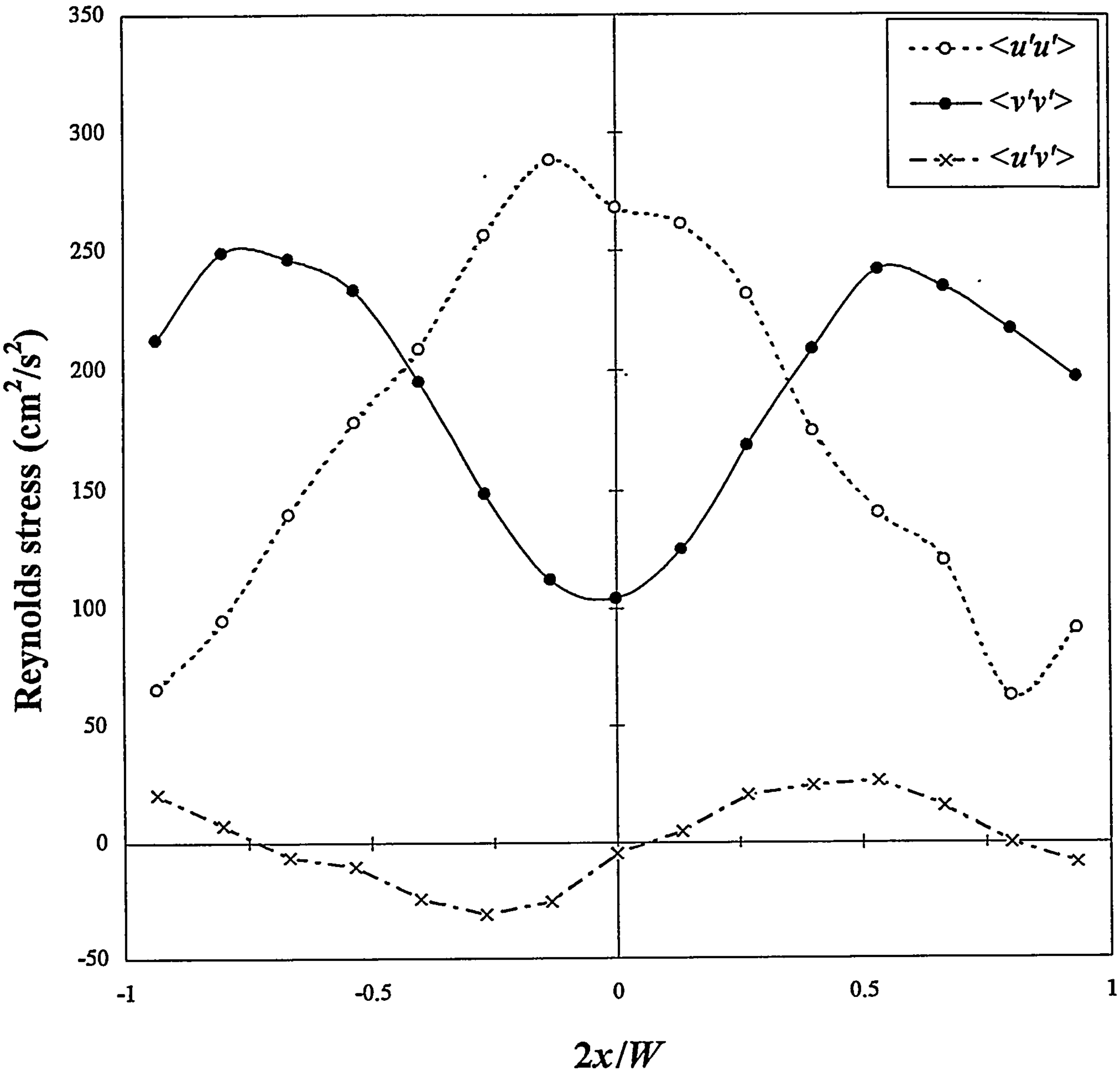

Figure 3. Profiles of the Reynolds stresses component for the middle section of the 15 cm column at U_{sup} = 1.0 cm/s.

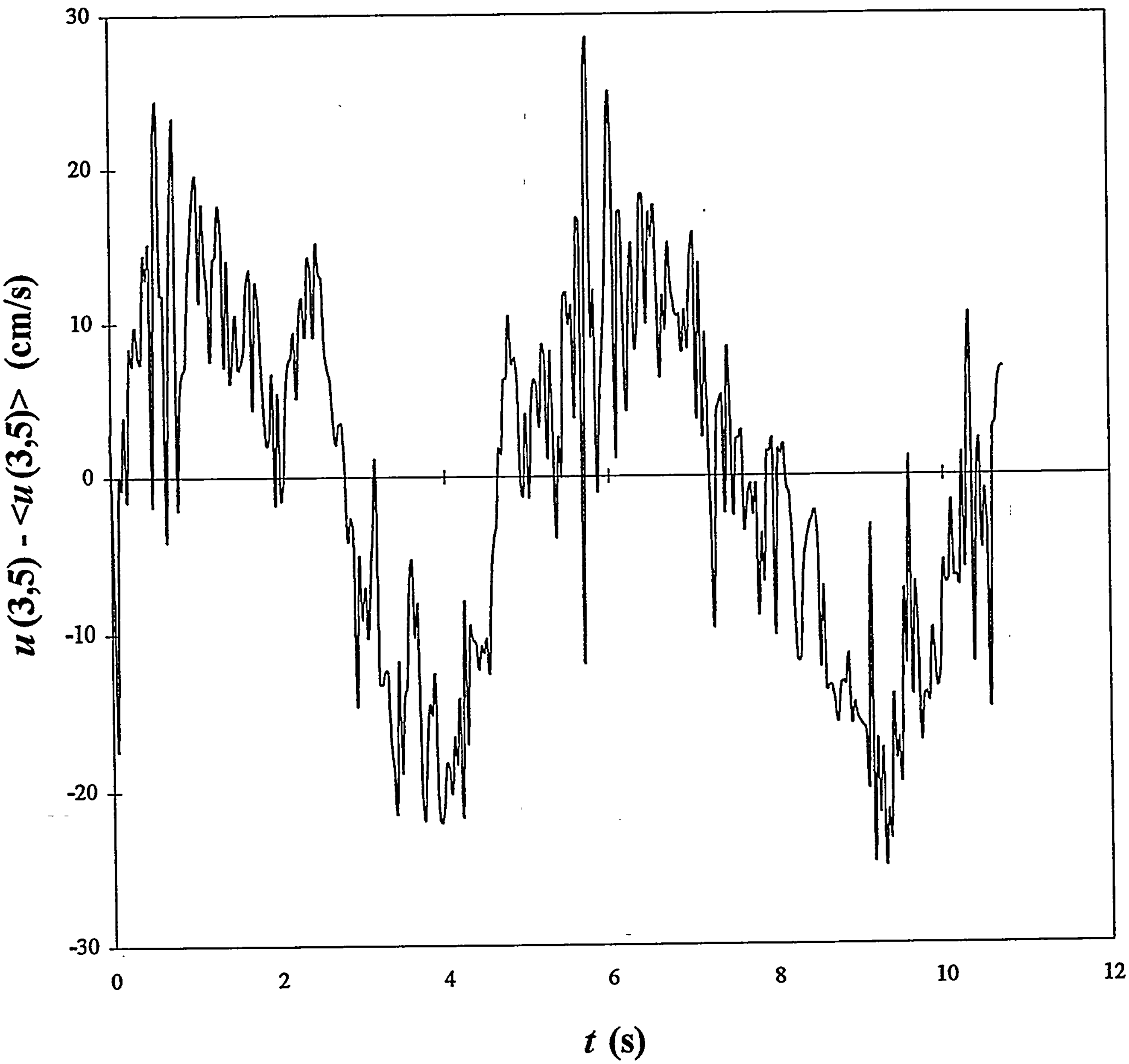

Figure 4a. Time series of the fluctuating component of the horizontal velocity of cell (3,5).

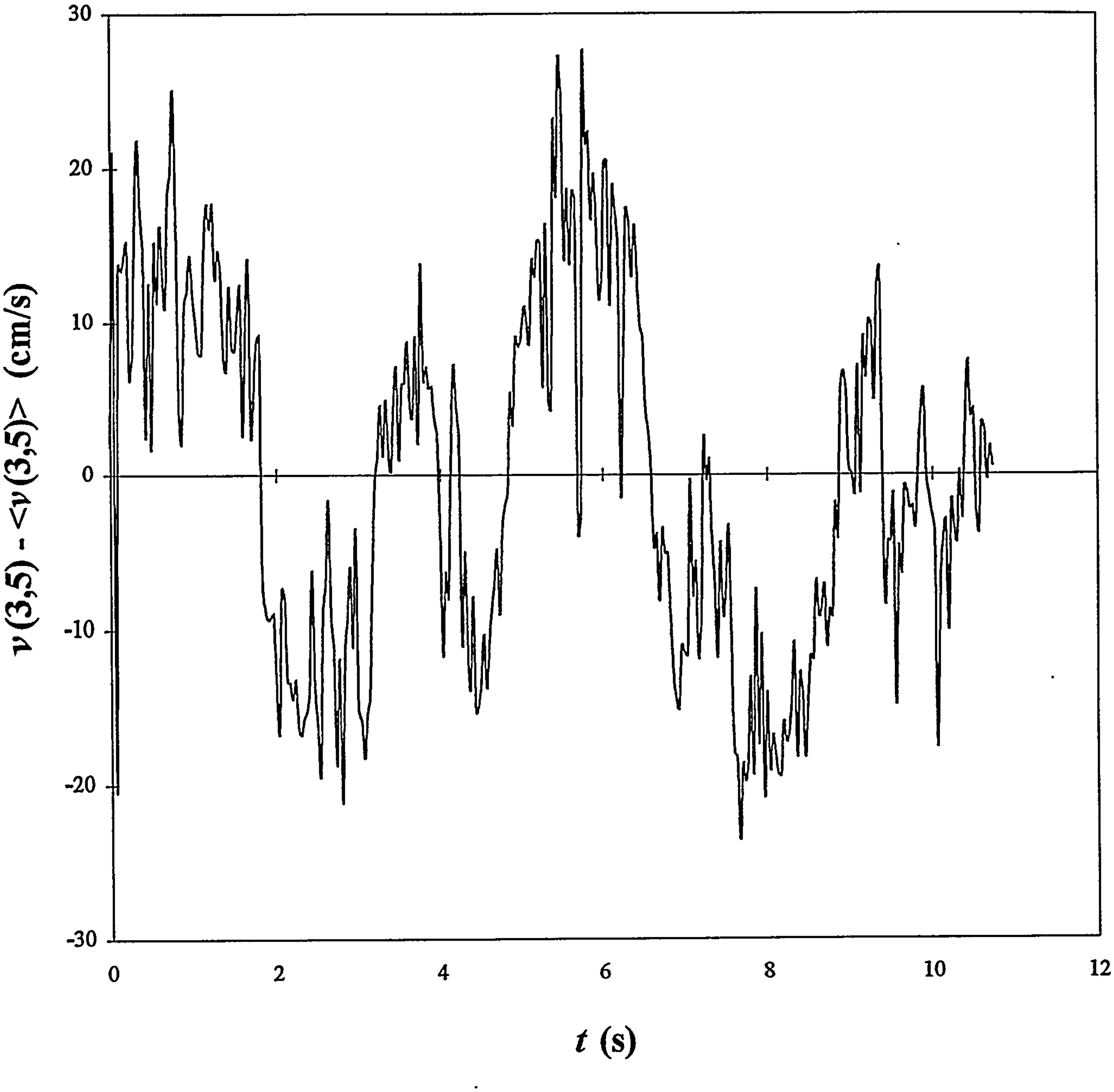

Figure 4b. Time series of the fluctuating component of the vertical velocity of cell (3,5).

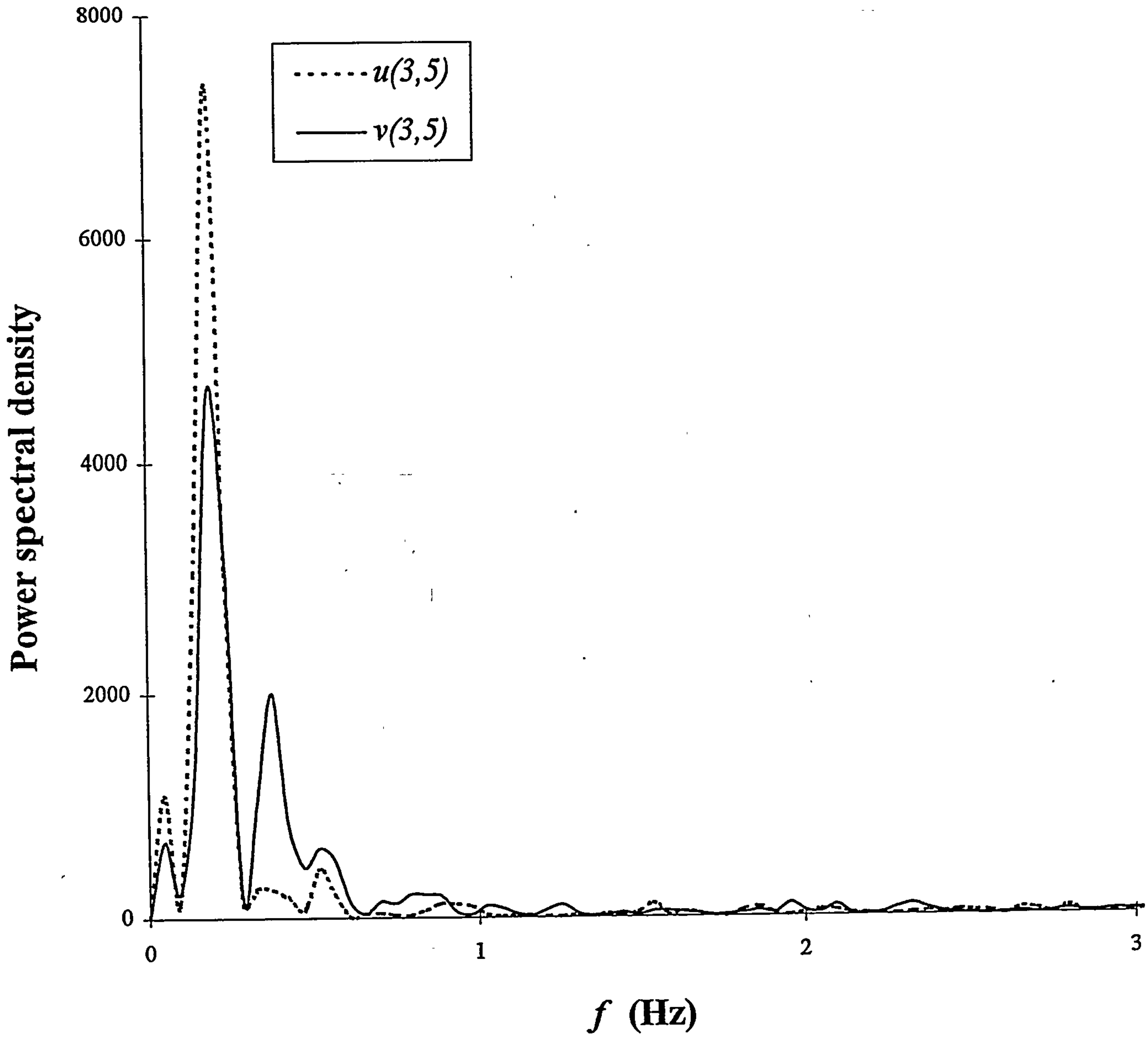

Figure 5. Power spectrum of the series shown in Figures 10a and 10b.

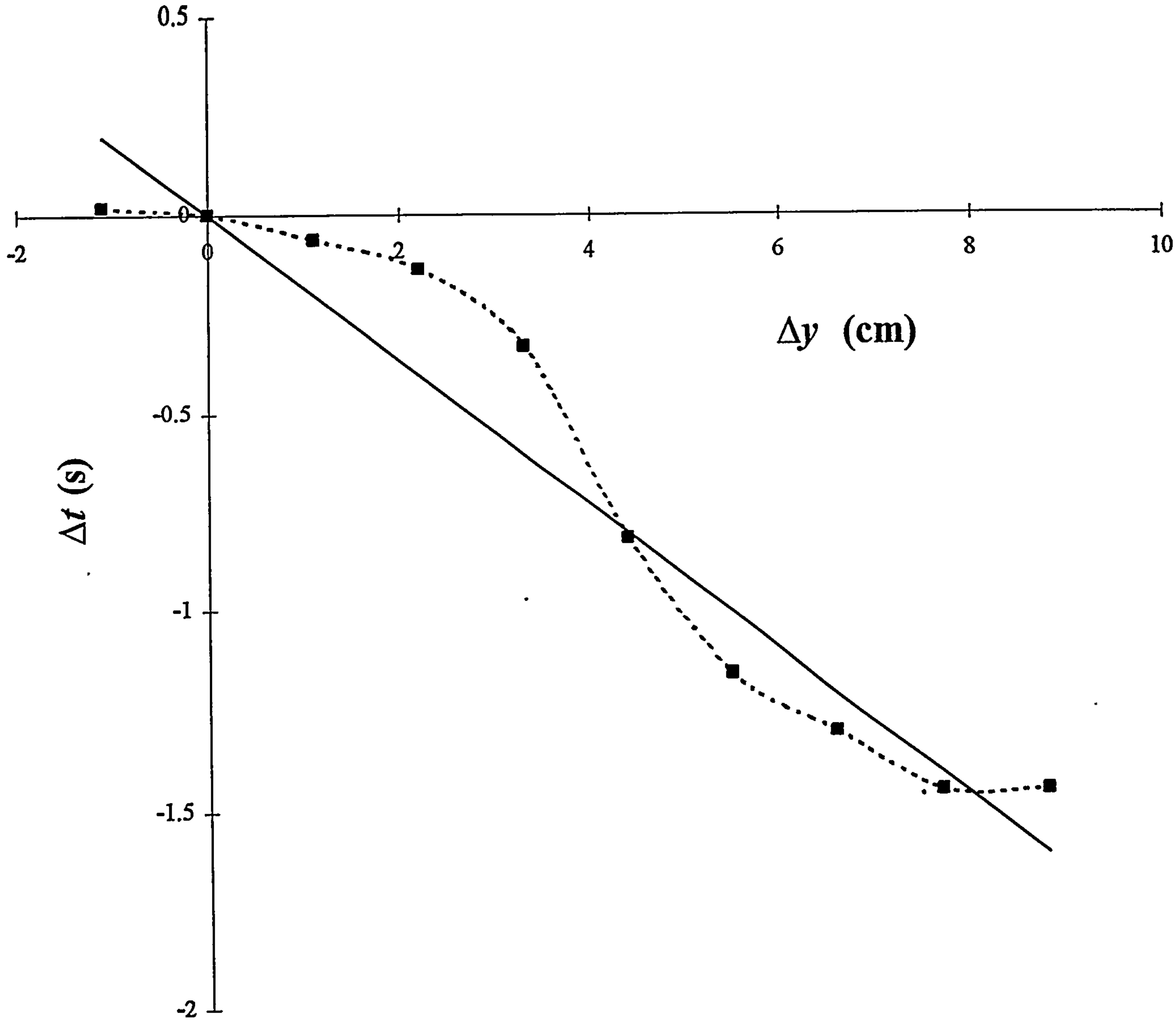

Figure 6. Time shift obtained from cross-correlating $v(2,2)$ and $v(2,j)$ as a function of the distance between the corresponding grid cells.

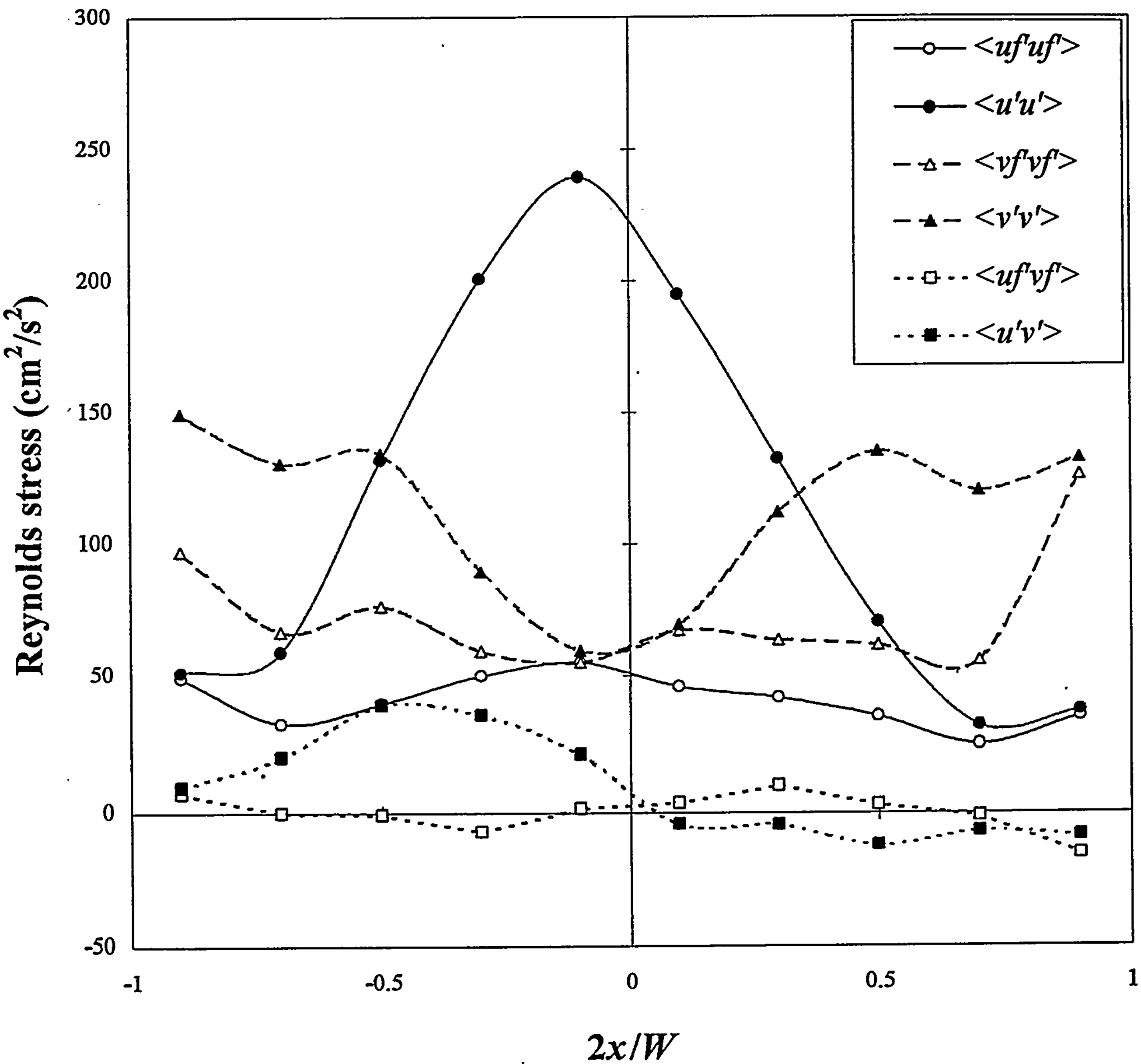

Figure 7. Reynolds stresses for the time series: high frequency fluctuations (open symbols) and total velocity (closed symbols).

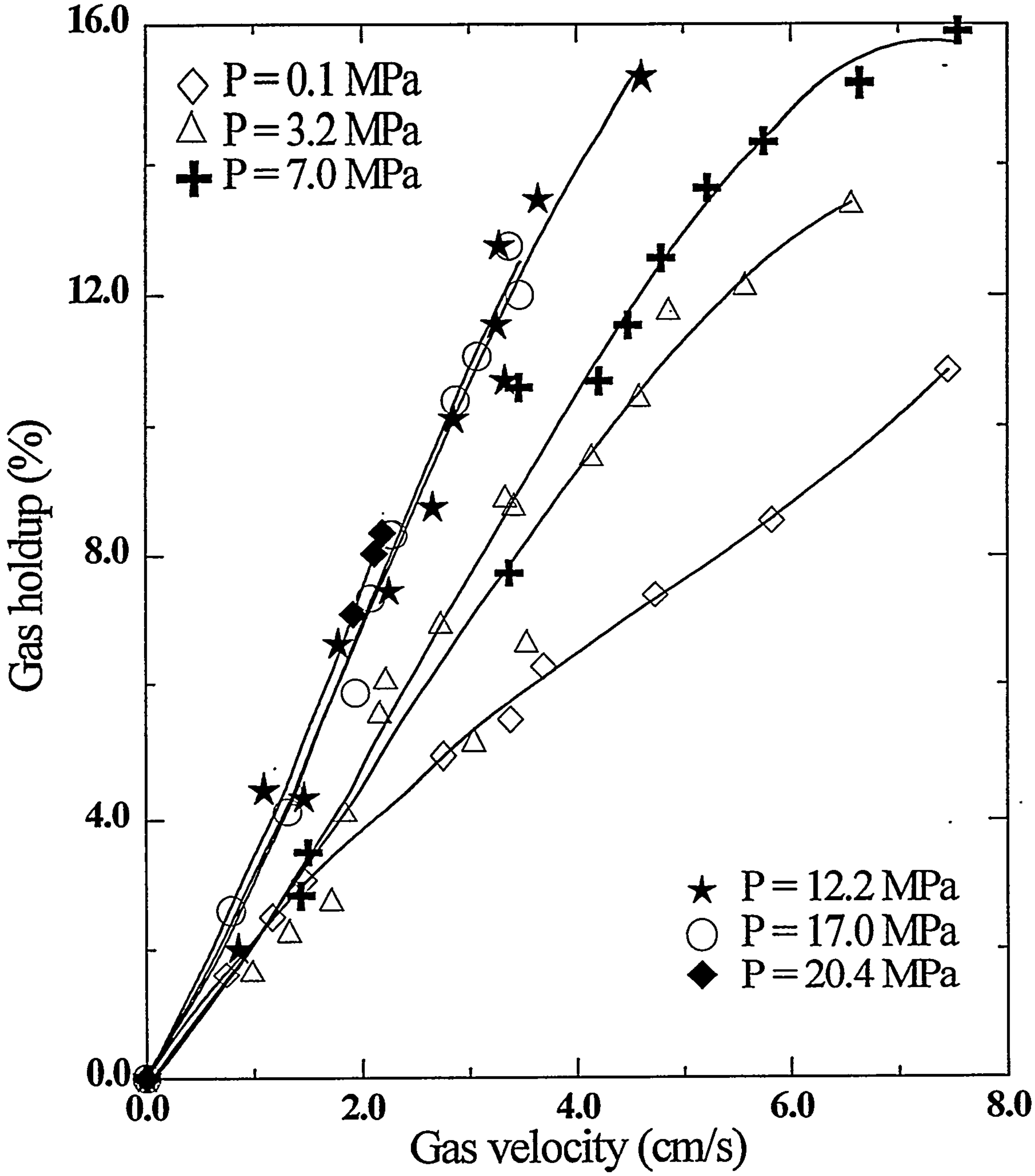

Figure 8. Effects of gas velocity on the gas holdup at various pressures (T = 25 °C).